Numerical simulation of the 3D behavior of thermal buoyant airflows in pentahedral spaces

El Hassan Ridouane *, Antonio Campo

Department of Mechanical Engineering, The University of Vermont, 33 Colchester Avenue, 201 Votey Building, Burlington, VT 05405, USA

ABSTRACT

A numerical study of three-dimensional natural convection in an attic space with heated horizontal base and cooled upper walls is presented. Every previous study pertinent to this subject as of today has assumed that the flow in attics is two-dimensional and restricted to triangular cavities. This problem is examined for fixed aspect ratios holding width to height of 2 and depth to height of 3.33 and Rayleigh numbers ranging from 10^4 to 8×10^5. The coupled system of conservation equations, subject to the proper boundary conditions, along with the equation of state assuming the air behaves as a perfect gas are solved with the finite volume method. In the conservation equations, the second-order-accurate QUICK scheme was used for the discretization of the convective terms and the SIMPLE scheme for the pressure-velocity coupling. It is categorically found that the flow in the attic is 3D. From the physics of the problem, two steady-state solutions are possible. The symmetrical solution prevails for relatively low Rayleigh numbers. However, as the Ra is gradually increased, a transition occurs at a critical value Ra_C. Above this value of Ra_C, an asymmetrical solution exhibiting a pitchfork bifurcation arises and eventually becomes steady. Results are presented detailing the occurrence of the pitchfork bifurcation and the resulting flow patterns are described.

© 2008 Elsevier Inc. All rights reserved.

1. Introduction

Natural convection in triangular enclosures has been an attractive field for researchers in the broad area of heat and fluid flow for more than two decades because many engineering systems can be accommodated into these closed configurations. Typical examples include attics of houses and buildings, electronic equipment cabinets and others. The first works devoted to the isosceles triangular geometry were concentrated on laminar flows and the majority of them were completed with considerable success. Focusing on the attic applications, two different scenarios are possible depending on the season of the year. In the wintertime, the attic is heated at the base and symmetrically cooled at the top inclined walls, whereas in the summertime, the attic is cooled at the base and symmetrically heated at the top inclined walls.

A literature review concerning isosceles triangular cavities shows that this configuration was the object of limited experimental and numerous numerical studies. In the early years, the flow and temperature patterns, local wall heat fluxes and mean heat flux rates were measured experimentally by Flack (1979, 1980) considering three different aspect ratios. The cavities filled with air, were heated/cooled from the base and cooled/heated from

the top inclined walls covering a wide range of Grashof numbers. Akinsete and Coleman (1982) conducted a numerical study based on the finite-difference method on natural convection flow of air contained in a right triangular cavity (half of the isosceles triangular cavity) with a cold base, heated top inclined wall and insulated vertical wall. Numerical solutions were obtained for height-to-base ratios ⩽0.5 in conjunction with Grashof numbers varying up to a maximum value of 8000. Poulikakos and Bejan (1983) reported a theoretical and numerical investigation of natural convection inside a right triangular cavity with cold inclined wall, warm base and insulated vertical wall. The theoretical flow and temperature fields were determined on the basis of an asymptotic analysis valid for shallow spaces with aspect ratios approaching zero. Another phase of the investigation focused on the temporal evolution of the flow and temperature fields for various aspect ratios of the cavity in question.

Using a numerical procedure based on the finite-element method, Del Campo et al. (1988) examined natural convection in an entire cavity for several combinations of thermal boundary conditions. For the particular case of heating from below and cooling from above, the computed velocity and temperature fields at low Grashof numbers were found to be symmetrical with respect to the mid-plane of symmetry in a cavity having unitary aspect ratio. Salmun (1995) examined a two-dimensional right triangular cavity filled with air or water covering various aspect ratios and

* Corresponding author. Tel.: +1 802 656 3304; fax: +1 802 656 1929.
E-mail address: eridouan@uvm.edu (El H. Ridouane).

Rayleigh numbers. The governing equations written in transient form were solved numerically and the obtained results were confirmed using two independent methods. The numerical simulations conducted showed that the single-cell circulation is not stable in the parametric domain considered. This solution breaks down as the Rayleigh number surpasses 3×10^3 and a new steady-state is achieved, i.e., that of a multi-cellular type. Asan and Namli (2000) conducted a numerical analysis of laminar natural convection in a pitched roof of triangular cross-section considering an adiabatic mid-plane wall condition. Only summertime conditions were considered over combinations of the Rayleigh number and the height-based aspect ratio. Their results showed that most of the heat exchange takes place near the intersection of the active walls.

The finite-element-method was used by Holtzman et al. (2000) to model the complete isosceles triangular cavity without claiming cavity symmetry. A heated base and symmetrically cooled top inclined walls were prescribed as thermal boundary conditions for various aspect ratios and Grashof numbers. These authors also performed a flow visualization experiment to validate the existence of symmetry-breaking bifurcations in one cavity of fixed aspect ratio. This anomalous bifurcation phenomenon was intensified by gradually increasing the Grashof number. The main conclusion drawn in this paper was that for identical isosceles triangular cavities engaging symmetrical and non-symmetrical assumptions, the mean Nusselt number differences were about 5%. It is worth adding that the majority of works cited above have assumed the existence of a vertical plane of symmetry passing through the middle of the isosceles triangular cavity in order to deal with a manageable computational domain that equates to half the size of the physical domain. Two years later, assuming a symmetrical nature of the flow within an attic space, Haese and Teubner (2002) investigated the thermal effects in building attics involving ceiling fans. The problem was solved for the winter condition implementing the vorticity-stream function formulation. Ridouane and Campo (2005) generated experimental-based correlations for the reliable characterization of the center plane temperature and the mean convective coefficient in isosceles triangular cavities filled with air. The experimental data was gathered from various sources for different combinations of aspect ratios and Grashof numbers. Ridouane et al. (2005) conducted numerical simulations of compressible air confined to an isosceles triangular cavity with a computational domain being coincident with the physical domain. The numerical results were compared against the experimental data measured by Flack (1979, 1980) for the two relevant cases corresponding to summer and winter situations. Good agreement was confirmed between the numerical predictions and the experimental measurements.

The heat transfer benefits derivable from connecting the bottom and top walls of attic enclosures with insulated vertical sidewalls were investigated numerically by Ridouane et al. (2006). Different heights of the insulated sidewalls were chosen varying from a limiting isosceles triangle cavity to a limiting rectangle cavity. The Prandtl number was set at 0.71 (for air), and values of the Rayleigh number within the range [10^3, 10^6] were assigned. The presence of insulated walls, even with a very small height, provides a huge gain of energy (for cooling in the summer or heating in the winter). More recently, transient thermal convection in an air-filled isosceles triangular cavity heated from below and cooled from above has been examined numerically by Ridouane and Campo (2006) over an extensive range of Grashof numbers. The influence of Gr on the flow and temperature patterns was analyzed and discussed for two contrasting scenarios, which correspond to increasing and decreasing Gr. Two steady-state solutions were obtained numerically using an appropriate set of initial perturbations. For increasing Gr, a sub-critical pitchfork bifurcation is created giving

rise to an anti-symmetric plume occurring at a critical Grashof number, $Gr_1 = 2 \times 10^5$. The evolution of the flow structure with time was generated in detailed form to illustrate how this physical transition manifests. Interestingly, the emergence of a hysteresis phenomenon is observed. Conceptually, this implies that the critical Gr characterizing the transition from one steady-state solution to another steady-state solution depends markedly on the scenario considered.

To the best knowledge of the authors, all the information available in the vast literature on fluid dynamics and natural convection transfer in the attic geometry is limited to 2D situations. Despite significant developments in the measurement techniques and instrumentation, as well as in the numerical methods with improved computing capacity, not a single 3D investigation has been reported. The objective of the present study is to fill this gap by performing detailed numerical simulations of 3D airflow in a pentahedral enclosure, which mimics the attic space of houses and buildings.

The paper is organized in sections, which successively present the mathematical and numerical formulation of the natural convection flow, the validation and accuracy of the numerical procedure, and finally the presentation and discussion of the new 3D results.

2. Modeling and governing equations

The physical system consists of a pentahedral cavity of height H, length $W = 2H$, and depth $L = 3.33H$ filled with air as shown in Fig. 1. The enclosed air is subject to a vertical gravitational field g $(0, -g, 0)$ where $g > 0$, with no-slip conditions at the walls. Initially, the air is in thermal equilibrium with the base and the two upper inclined walls maintained at a low temperature T_C. The other two vertical walls are insulated. At a pre-set time, the base is heated and maintained at a high temperature T_H while the two upper inclined walls stay at the low temperature T_C. We assumed that the air behaves as a perfect gas. The viscosity μ, specific heat capacity
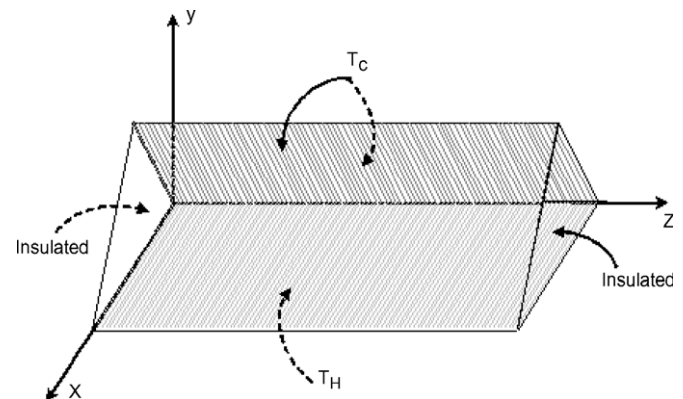

Fig. 1. Sketch of the pentahedral cavity.

Table 1
Sensitivity of the grid density in terms of the maximum velocity components and the mean Nusselt number at $Ra = 8 \times 10^5$

Grid size	u^*_{max}	v^*_{max}	w^*_{max}	Nu
609,268	264.53	370.25	293.19	100.59
807,259	260.72	362.54	308.26	99.65
914,582	258.09	356.07	317.85	98.81
1,306,726	256.16	350.44	322.52	98.69
2,375,019	255.71	350.12	321.18	98.75

C_p and thermal conductivity k are taken as constants and evaluated at the reference temperature $T_0 = (T_H + T_C)/2$. Under these circumstances, the three-dimensional versions of the Navier–Stokes equations and the energy equation, along with the ideal gas equation are

$$\frac{\partial \rho}{\partial t} + \text{div}(\rho \mathbf{u}) = 0 \tag{1}$$

$$\frac{\partial (\rho u)}{\partial t} + \text{div}(\rho u \mathbf{u}) = -\frac{\partial p}{\partial x} + \text{div}(\mu \, \text{grad} \, u) \tag{2}$$

$$\frac{\partial (\rho v)}{\partial t} + \text{div}(\rho v \mathbf{u}) = -\frac{\partial p}{\partial y} + \text{div}(\mu \, \text{grad} \, v) + (\rho - \rho_0)g \tag{3}$$

$$\frac{\partial (\rho w)}{\partial t} + \text{div}(\rho w \mathbf{u}) = -\frac{\partial p}{\partial z} + \text{div}(\mu \, \text{grad} \, w) \tag{4}$$

$$\frac{\partial (\rho e)}{\partial t} + \text{div}(\rho e \mathbf{u}) = -p \, \text{div} \mathbf{u} + \text{div}(k \, \text{grad} \, T) \tag{5}$$

$$p = \rho R T \tag{6}$$

$$e = C_v T \tag{7}$$

In Eqs. (1)–(5) the following notation has been adopted: x, y and z, are the coordinates; u, v and w, are the velocities components; p,
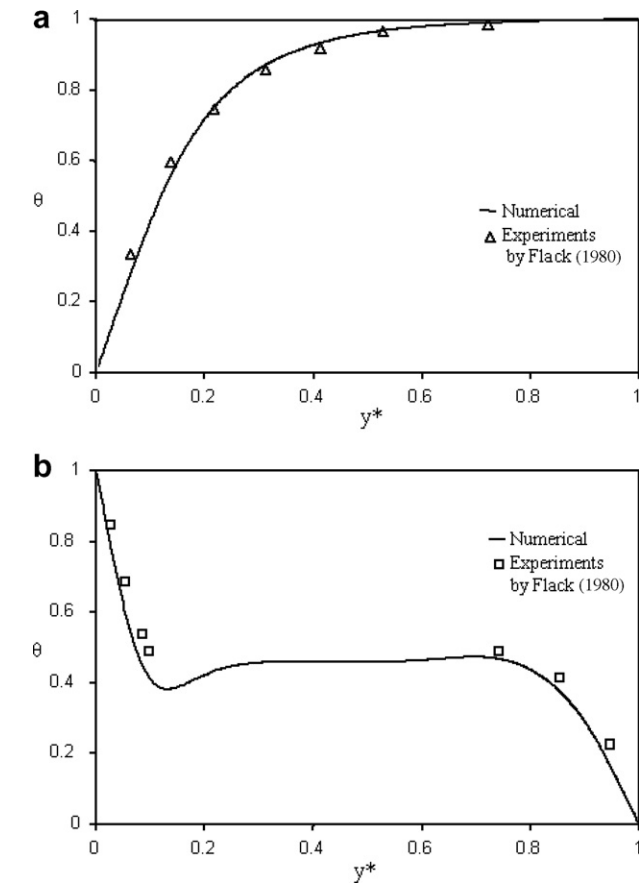
Fig. 2. Typical dimensionless centerline temperature profiles: (a) cavity heated from above and cooled from below and (b) cavity heated from below and cooled from above.

Table 2
Comparison against the benchmark data involving a differentially heated cubic cavity for $Ra = 10^5$

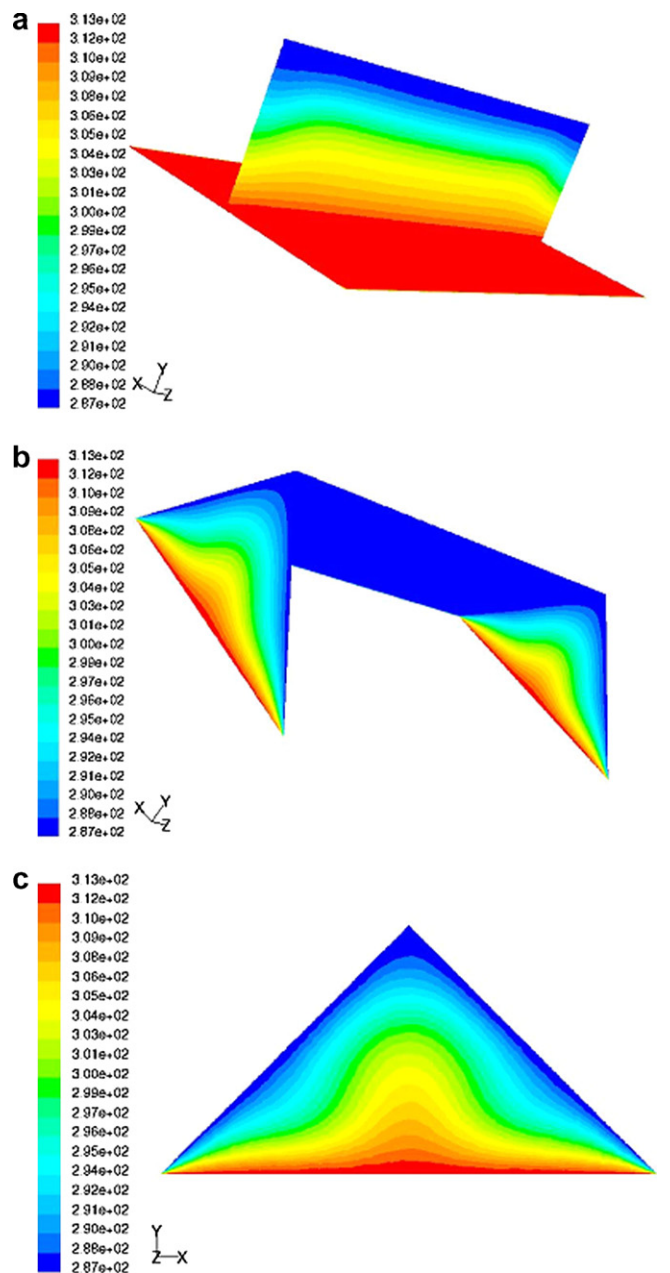|	Present work	Tric et al. (2000)
Grid	61^3	61^3
u^*_{max}	44.15	43.90
x^*	−0.18	−0.18
y^*	0.22	0.22
z^*	0.38	0.39
v^*_{max}	9.80	9.69
x^*	0.41	0.42
y^*	0.34	0.34
z^*	0.37	0.38
w^*_{max}	71.49	71.06
x^*	0.43	0.43
y^*	0.38	0.37
z^*	0.008	0.006
$u^*_{mp,max}$	43.50	43.06
x^*	−0.18	−0.19
z^*	0.37	0.38
$w^*_{mp,max}$	66.38	65.43
x^*	0.42	0.43
z^*	0.016	0.010
Nu_{mp}	4.52	4.61

Fig. 3. Symmetrical steady-state isotherms at low $Ra = 10^4$: (a) at the mid-plane $x^* = 0.5$, (b) at the insulated walls, and (c) at the mid-plane $z^* = 0.5$.
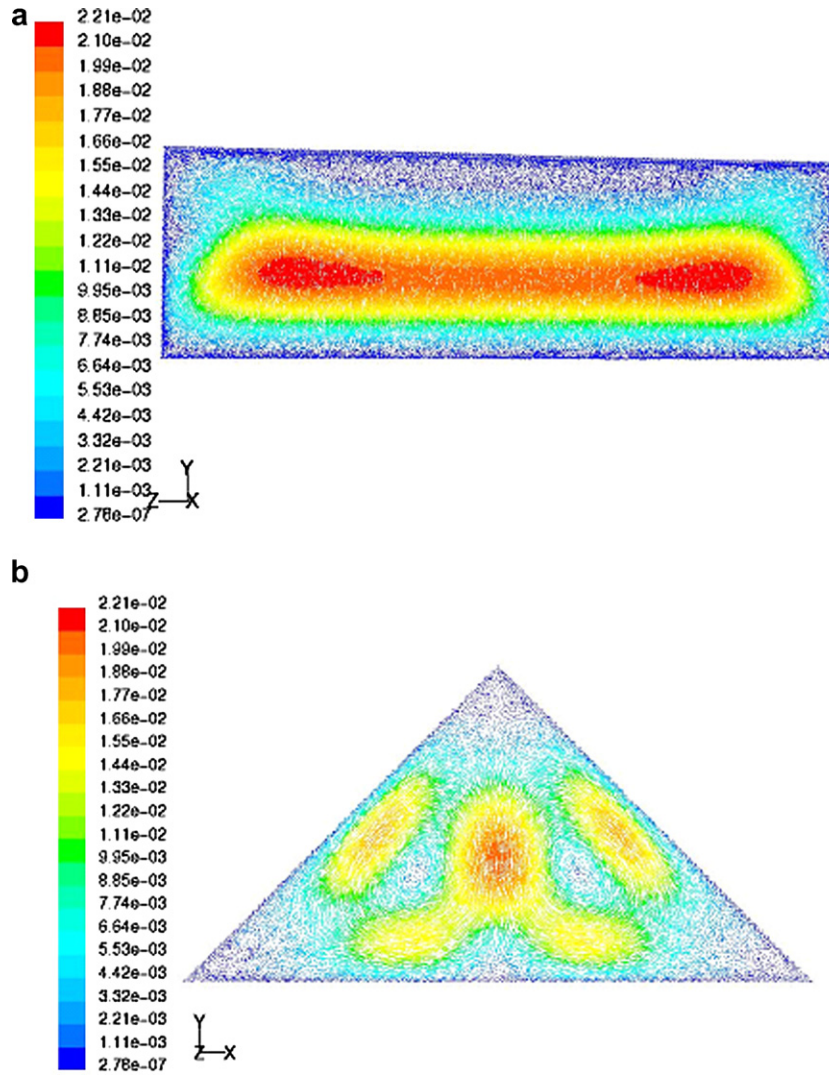
Fig. 4. Symmetrical steady-state velocity vectors at low $Ra = 10^4$: (a) at the mid-plane $x^* = 0.5$ and (b) at the mid-plane $z^* = 0.5$.

static pressure; T, temperature; ρ, the density and ρ_0, the density evaluated at the reference temperature T_0; R, the ideal gas constant; e, the internal energy.

3. Numerical method

The computational domain is constructed to be coincident with the physical domain forming the pentahedral space. The governing Eqs. (1)–(5), along with the ideal gas equation of state (6) subject to the boundary and initial conditions are solved implementing the finite volume method (Tannehill et al., 1997). The fully implicit discretization approach was used for discretizing the transient equations on the grounds of its superior stability. The discretization of the momentum and energy conservation equations was carried out with the QUICK scheme. The density in the equation of state was handled by a second-order upwind scheme. A second-order body-force-weighted scheme was utilized in the pressure discretization and the SIMPLE scheme was employed in the pressure-velocity coupling. Convergence to the final steady-state was assessed through monitoring the computed residuals in the energy, momentum and mass conservation equations by setting its variations to less than 10^{-6}. Also, through the convergence of point

and/or surface monitors for velocity, temperature and heat flux at selected locations within the computational domain.

For the sake of generality, taking H^2/α as the time scale, we define the dimensionless time as
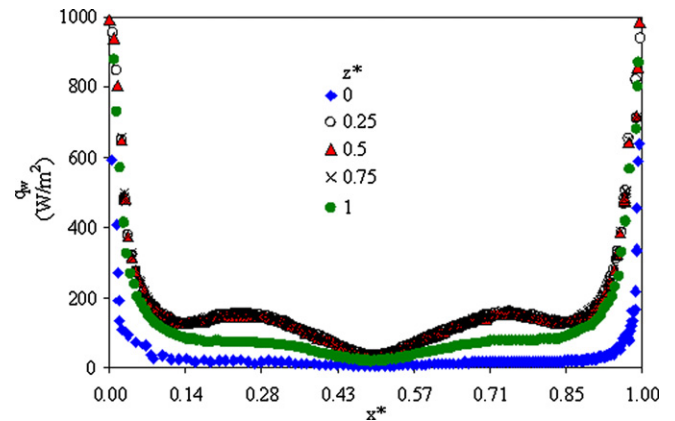

Fig. 5. Local heat flux along the x-direction on the hot base for different cavity depths sharing $Ra = 10^5$.

$$\tau = \frac{t}{H^2/\alpha} \qquad (8)$$

with α the air thermal diffusivity in the preceding ratio. A fixed time step $\Delta\tau$ of 1.3×10^{-4} is considered for all numerical experiments.

A sensitivity study was performed to analyze the influence of the mesh spacing on the final steady-state velocity and temperature results. Five different staggered grid sizes ranging from 609,269 to 2,375,019 tetrahedral control volumes were tested at a high Rayleigh number of 8×10^5. The items listed in Table 1 indicate how the maxima of the dimensionless velocity components ($u^* = uH/\alpha$, $v^* = vH/\alpha$, $w^* = wH/\alpha$) and mean Nusselt number in the 3D cavity converge with the grid refinements. As the number of grid elements increase, each quantity converges towards a given value. Based on these numerical experi-

ments, it was decided that the grid with 1,306,726 elements is the optimal computational mesh, which can be used with confidence to generate all the numerical results in this study. The mesh was constructed to be symmetrical with respect to the mid-plane of the cavity. Care was taken as to increase the element density in sensitive areas where pronounced velocity and temperature gradients would occur, such as near the bounding walls. In reference to this, special emphasis was placed at the wall intersections. In fact, there is a temperature discontinuity at the two lower corners of the cavity, which necessitated high grid density to predict the temperature and velocity fields in these regions.

Two validations of the numerical code developed to solve the governing equations for the natural convection problem were done. A first validation dealt with the 2D experimental temperatures measured by Flack (1980) for air under steady-state conditions. Among the three isosceles triangular cavities tested in Flack (1980), we chose the one holding an intermediate apex angle of 45° between the base and the top inclined walls as representative to carry out the comparison. Fig. 2a displays the variation of the computed dimensionless temperature $\theta = (T - T_C)/(T_H - T_C)$ along the mid-plane of the isosceles triangular cavity symmetrically heated from the top inclined walls and cooled from the base for the highest Grashof number $Gr = 2.84 \times 10^6$ selected by Flack (1980). It is observable in the figure that the air is nearly isothermal in the upper part of the cavity between the locations $y^* = 0.6$ and 1 ($y^* = y/H$). This signifies that the heat is transferred by conduction in this region. When compared against the experimental observations of Flack (1980), the numerical temperatures exhibit the correct trends and more important the agreement is excellent. In addition, for the cavity heated from below and cooled from above, the center plane temperature profiles are presented in Fig. 2b for $Gr = 6.25 \times 10^5$. In this figure, large temperature drops are manifested near the top and bottom of the cavity, i.e., in the segments occupied by $y^* < 0.2$ and $y^* > 0.8$. The remaining central portion of the cavity stays isothermal around a constant dimensionless temperature $\theta = 0.5$. The concordance between the numerical and experimental temperatures is deemed adequate. A second validation was carried out against the 3D benchmark results in a differentially heated cubic cavity at $Ra = 10^5$ reported by Tric et al. (2000). Table 2 illustrates the comparison of the following quantities: (a) the maximum of each dimensionless velocity component in the cavity with its location; (b) the maximum of u^* and w^* in the mid-plane ($y^* = 0$) with their locations, and (c) the mean Nusselt number at the mid-plane Nu_{mp}. Excellent agreement was observed between the two sets of results owing maximum differences within a 2% band.

4. Results

The collection of 3D numerical simulations performed for air ($Pr = 0.71$) and Rayleigh number varying from 10^4 to 8×10^5 is conducive to a parametric study. In all numerical results to be presented, a constant temperature difference (T_H–T_C) of 26 K has been imposed between the hot base and the two equally cold top inclined walls.

Symmetrical steady-state solutions are observed at low Ra numbers, which are characterized by two counter rotating cells. As Ra progressively increased, a transition to an asymmetrical steady-state is manifested at a critical value of Rayleigh number Ra_C. A special effort is made here to illustrate the flow and temperature patterns in the whole cavity volume as the Rayleigh number changes. Convincing evidence is provided to the fact that the flow in attics is 3D and the 2D assumption fails as Ra exceeded a critical value.
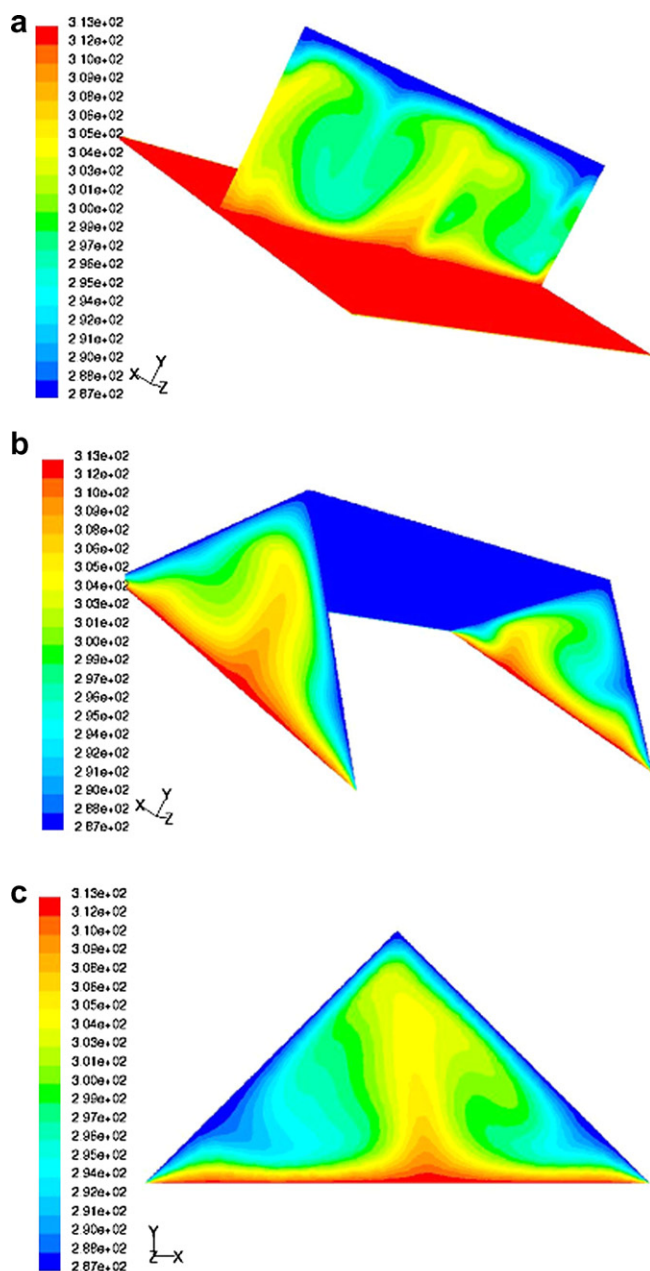

Fig. 6. Steady-state isotherms at $Ra_C = 1.45 \times 10^5$ just after the transition from symmetrical to asymmetrical conditions.
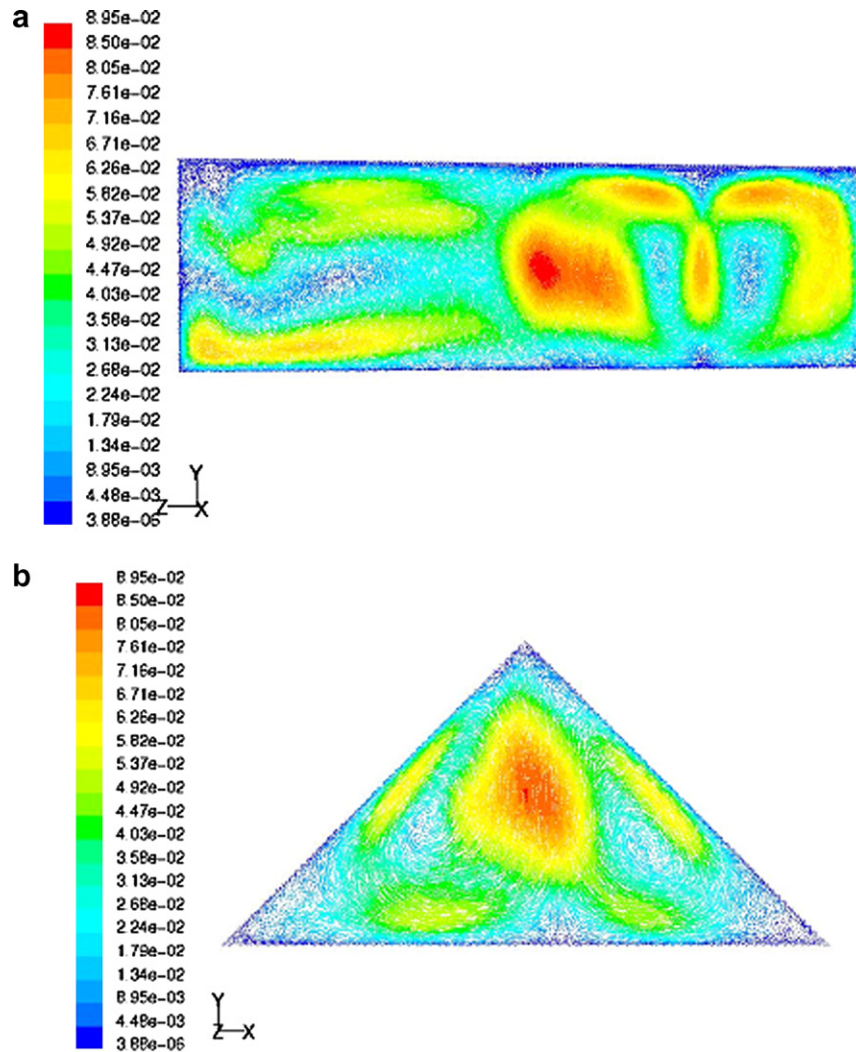
Fig. 7. Distribution of the steady-state velocity vectors at $Ra_C = 1.45 \times 10^5$: (a) on the mid-plane $x^* = 0.5$, and (b) on the mid-plane $z^* = 0.5$.

4.1. symmetrical patterns

Transient calculations were conducted at low Ra numbers starting from rest as initial conditions. The final steady-state solution is symmetrical with respect to the geometrical mid-planes $x^* = x/W = 0.5$ and $z^* = z/L = 0.5$. For all velocity vectors and isotherm plots, the labels are provided with dimensional format (in m/s for velocity vectors and in K for isotherms). Typical symmetrical solutions are illustrated in Fig. 3 at $Ra = 10^4$ and consists of isotherms plotted on the plane $x^* = 0.5$ (Fig. 3a), on the insulated walls $z^* = 0$ and $z^* = 1$ (Fig. 3b), and on the plane $z^* = 0.5$ (Fig. 3c). The fluid circulation is slow and characterized by two long vortices rotating in opposite directions, which accommodate to the shape of the geometry. When examining (Fig. 3b and c), it is clear that the flow structure stays almost unaltered with respect to the *z-direction at this low Ra number*. The corresponding velocity vectors are presented in Fig. 4a and b on the mid-planes $x^* = 0.5$ and $z^* = 0.5$, respectively. The region of high fluid velocity is observed in the center of the cavity between the two vortices; this region is shaped as a cylinder along the *z*-direction. On the contrary, the regions of intermediate velocities are located near the walls and far from the corners.

Heat flux results for symmetrical steady-states are presented in terms of the local heat flux curves on the hot wall along the *x*-direction. Fig. 5 illustrates the magnitude of the local wall heat flux q_w at $Ra = 10^5$ for different cavity depths. For small values of x^*, q_w begins with a relatively large value at the point where the temperature discontinuity occurs, i.e., at $x^* = 0$. This behavior is due to the important heat transfer by conduction in these regions because of the small separation between the hot and cold walls. As x^* grows, q_w exhibits a concave U-shaped path with respect to the abscissa x^*. In the large sub-interval $0.1 \leqslant x^* \leqslant 0.9$, q_w stays almost constant showing subtle variations. This comportment responds to the fact that considerable thermal convection has occurred. Further, except for the two extreme curves related to $z^* = 0$ and 1, it is obvious that the q_w curves are identical inside the cavity. This similitude confirms the symmetrical nature of the flow. The fact that the distribution of q_w at $z^* = 0$ and 1 is different for the distribution within the cavity is attributed to the effects of the vertical insulated walls located in these two positions.

4.2. Transition

The initialization of the calculations for a higher Rayleigh number is taken from the previous steady-state solution. For instance, the initialization for $Ra = 10^5$ is taken from the steady-state solution of $Ra = 5 \times 10^4$. By increasing Ra from 10^4, which is associated with the steady-state solution depicted in Fig. 3, no visible

qualitative change was observed in the shape of the vortices. However, quantitatively, the intensity of the flow is invigorated. This action improves the overall heat transfer through the upper cold walls of the pentahedral cavity. The buoyant flow stays steady for a wide range of Ra, but as Ra was gradually increased the symmetric patterns disappears and a sub-critical pitchfork bifurcation is created at a critical value of Rayleigh number, say Ra_C. Above this Ra_C value, asymmetric patterns appear. These remain steady for a wide range of Ra even if the initial conditions are those associated with the symmetrical flow.

Special efforts have been made to determine this critical value Ra_C with 1% as maximum relative error. The tests were conducted by increasing Ra from 10^5 with very small steps when necessary, but it was found that the steady-state solutions were symmetrical until Ra reaches the critical value $Ra_C = 1.45 \times 10^5$. As the compu-

tational time τ increases, the flow visualization at Ra_C reveals that minor flow deformations are observed when τ reaches the value of 2.54. At this instant, the right vortex has increased and passed the mid-plane while the left vortex remains in the corner but diminishes in size. This behavior intensifies with time until the flow patterns reach a new steady-state at $\tau = 5.07$. Further increments in time do not seem to affect the flow and temperature fields. To summarize, the final steady-state condition attained at $Ra = 1.45 \times 10^5$ is depicted in Fig. 6.

The three-part figure exhibits the asymmetrical steady-state isotherms at the mid-plane $x^* = 0.5$ in Fig. 6a, at the insulated walls in Fig. 6b, and at the mid-plane $z^* = 0.5$ in Fig. 6c. It is evident here that the flow is not symmetrical with respect to both geometrical planes of symmetry. Fig. 6a shows the fluid plumes in the z-direction as they are moving up from the hot wall carrying the hot fluid to the upper regions of the cavity. The 3D effects of the flow patterns are pronounced; multiple vortices with different sizes exist inside the cavity. These vortices are not organized with respect to any symmetry plane of the geometry. The isotherms of Fig. 6b reveal that the flow structures at the two insulated walls are similar. The vortices switch the location and direction when going from one wall to the other. The velocity vectors of Fig. 7 are connected to the steady-state condition taken at Ra_C giving additional information about the velocity distribution in the attic just after the transition. Multi-vortices structure is observed with vortices rotating in all directions while in the symmetrical state the flow was organized holding two long vortices only.

4.3. Asymmetrical patterns

As Ra is increased further above Ra_C, the flow patterns become increasingly asymmetric and the number of secondary vortices tends to increase. These secondary vortices take over the space occupied by the main vortices as evidenced in Fig. 8 at $Ra = 8 \times 10^5$. The direct effect of the secondary vortices on the temperature field can be seen in Fig. 8a, where several streams of warm air are diverted upward and away from the wall. These new vortices move warm air up from the bottom and help intensify the heat transfer from the base. Fig. 9 illustrates the flow pattern resulting from the vortical structure at the mid-planes $x^* = 0.5$ in Fig. 9a and $z^* = 0.5$ in Fig. 9b for the same Rayleigh number cited above. Compared to the situation with $Ra = 1.45 \times 10^5$ depicted in Fig. 7, its is evident that in addition to a reduced size of the vortices, the magnitude of the velocity vectors inside the cavity increased resulting in higher vortices strength. Interestingly, the velocity vectors distribution at the $z^* = 0.5$ plane in Fig. 9b is almost symmetrical and characterized by two vortices with very thin boundary layers.

The 3D effects upon the heat transfer activity for asymmetrical steady-states are presented by way of the variations of the local heat flux along the axis of symmetry of the hot wall ($x^* = 0.5$ and $y^* = 0$). This outcome is displayed in Fig. 10 for $Ra = 8 \times 10^5$. The evolution of q_w with the dimensionless depth z^* emphasizes how the fluid at the boundary layer carries heat away from this region of the wall. Here q_w begins with a low value at the insulated vertical wall located at $z^* = 0$. As the distance along the wall increases, the heat transferred from the wall varies. q_w passes through maxima and minima before reaching the other insulated wall at $z^* = 1$ with the same value as it began with at $z^* = 0$. The minima of q_w occur in the regions of the wall corresponding to the areas between the vortices where the fluid is diverted from the wall. In this regards, the amplitudes of the maxima are proportional to the vortices strengths. The maximum related to the highest peak is located around $z^* = 0.3$ where the thinnest thermal boundary layer exists as can be seen in the isotherm plots appearing in Fig. 8a.
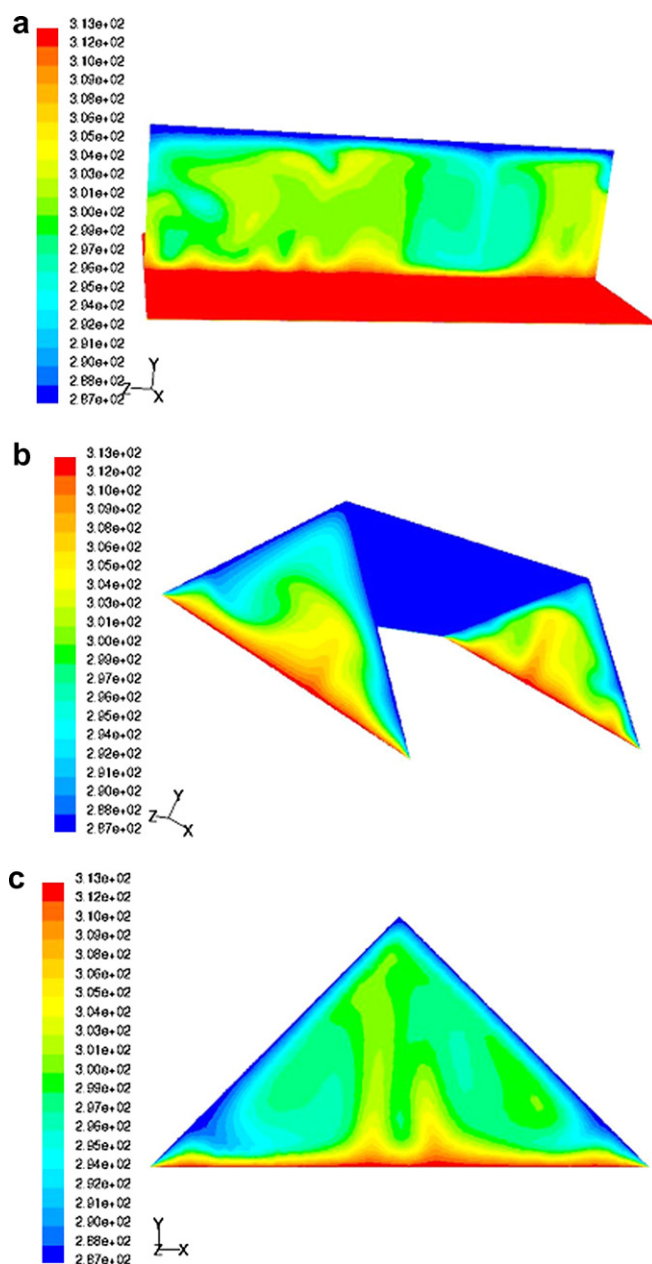

Fig. 8. Asymmetric steady-state isotherms at high $Ra = 8 \times 10^5$: (a) at the mid-plane $x^* = 0.5$, (b) at the insulated walls, and (c) at the mid-plane $z^* = 0.5$.
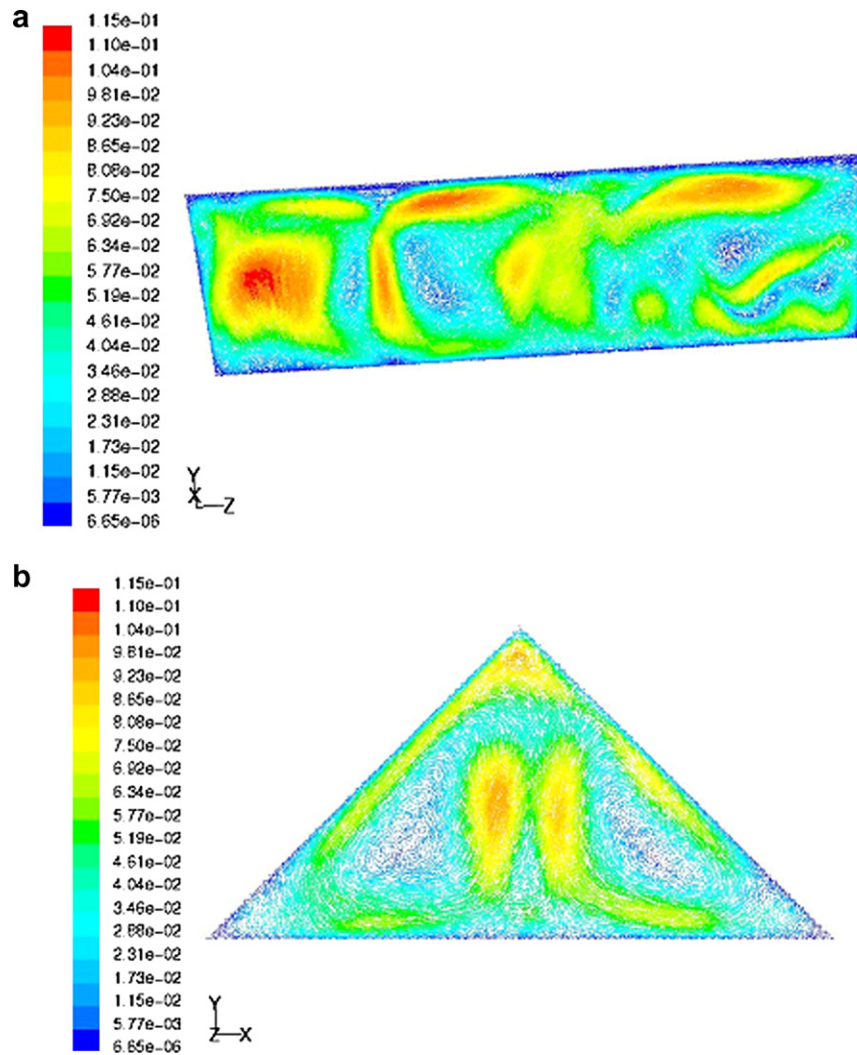
Fig. 9. Asymmetric steady-state velocity vectors for a high $Ra = 8 \times 10^5$: (a) at the mid-plane $x^* = 0.5$ and (b) at the mid-plane $z^* = 0.5$.
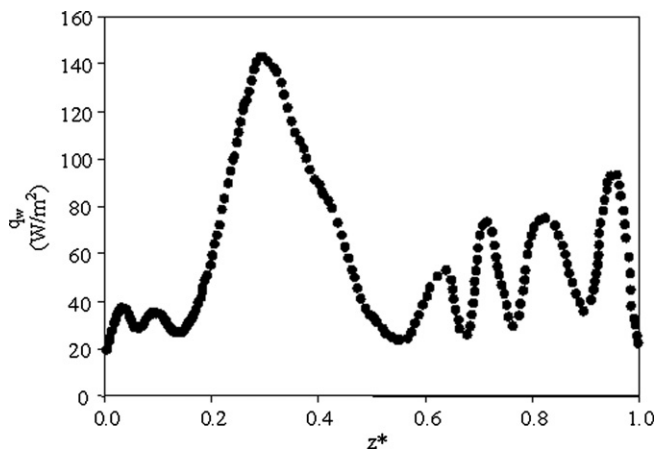

Fig. 10. Evolution of the asymmetric steady-state local heat flux at the hot base with the cavity depth along the center-line ($x^* = 0.5$, $y^* = 0$) when $Ra = 8 \times 10^5$.

5. Concluding remarks

Transient 3D thermal convection in an air-filled pentahedral cavity, which mimics the attic space of houses, has been studied numerically for wintertime conditions. During the winter season the attic is heated from the base and cooled from above inclined walls. This problem is examined for fixed aspect ratios holding width to height of 2 and depth to height of 3.33 and Rayleigh numbers ranging from 10^4 to 8×10^5. To perform the computational analysis, the finite volume method is used for the discretization of the governing conservation equations. Multiple steady-state solutions were obtained numerically using appropriate initial perturbations. For increasing Ra, it is confirmed that the symmetrical flow is achievable at relatively low Ra numbers. However, as Ra is continually augmented, the symmetric plume breaks down and fades away. Thereafter, a sub-critical pitchfork bifurcation is created giving rise to an anti-symmetric plume occurring at a critical Rayleigh number, $Ra_C = 1.45 \times 10^5$. It is demonstrated that the 2D assumption adopted by earlier studies dealing with fluid flow and heat transfer in attic spaces is not valid. The flow patterns are 3D for all the Rayleigh numbers considered ranging form 10^4 to 8×10^5.

References

Akinsete, V.A., Coleman, T.A., 1982. Heat transfer by steady laminar free convection in triangular enclosures. Int. J. Heat Mass Transfer 25, 991–998.
Asan, H., Namli, L., 2000. Laminar natural convection in a pitched roof of triangular cross section: Summer day boundary condition. Energy Build. 33, 69–73.

Del Campo, E.M., Sen, M., Ramos, E., 1988. Analysis of laminar convection in a triangular enclosure. Numer. Heat Transfer 13, 353–372.

Flack, R.D., 1979. Velocity measurements in two natural convection air flows using a laser velocimeter. J. Heat Transfer 101, 256–260.

Flack, R.D., 1980. The experimental measurement of natural convection heat transfer in triangular enclosures heated or cooled from below. J. Heat Transfer 102, 770–772.

Salmun, H., 1995. Convection patterns in a triangular domain. Int. J. Heat Mass Transfer 38, 351–362.

Holtzman, G.A., Hill, R.W., Ball, K.S., 2000. Laminar natural convection in isosceles triangular enclosures heated from below and symmetrically cooled from above. J. Heat Transfer 122, 485–491.

Haese, P.M., Teubner, M.D., 2002. Heat exchange in an attic space. Int. J. Heat Mass Transfer 45, 4925–4936.

Poulikakos, D., Bejan, A., 1983. The fluid mechanics of an attic space. J. Fluid Mech. 131, 251–269.

Ridouane, E.H., Campo, A., 2005. Experimental-based correlations for the characterization of free convection of air inside isosceles triangular cavities with variable apex angles. Exp. Heat Transfer 18, 81–86.

Ridouane, E.H., Campo, A., McGarry, M., 2005. Numerical computation of buoyant airflows confined to attic spaces under opposing hot and cold wall conditions. Int. J. Thermal Sci. 44 (10), 944–952.

Ridouane, E.H., Campo, A., Hasnaoui, M., 2006. Benefits derivable from connecting the bottom and top walls of attic enclosures with insulated vertical side walls. Numer. Heat Transfer Part A 49, 175–193.

Ridouane, E.H., Campo, A., 2006. Formation of a pitchfork bifurcation in thermal convection flow inside an isosceles triangular cavity. Phys. Fluids 18 (7), 074102.

Tannehill, J.C., Anderson, D.A., Pletcher, R.H., 1997. Computational fluid mechanics and heat transfer. Taylor and Francis, Washington, DC.

Tric, E., Labrosse, G., Betrouni, M., 2000. A First incursion into the 3D structure of natural convection of air in a differentially heated cubic cavity, from accurate numerical solutions. Int. J. Heat Mass Transfer 43, 4043–4056.